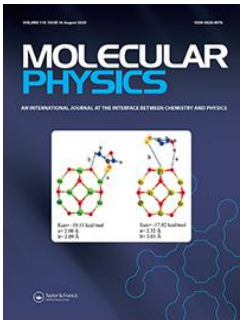

Taylor & Francis
Taylor & Francis Group

Molecular Physics

An International Journal at the Interface Between Chemistry and Physics

ISSN: (Print) (Online) Journal homepage: https://www.tandfonline.com/loi/tmph20

A rapid, spatially dispersive frequency comb spectrograph aimed at gas phase chemical reaction kinetics

Frances C. Roberts, H. J. Lewandowski, Billy F. Hobson & Julia H. Lehman

To cite this article: Frances C. Roberts, H. J. Lewandowski, Billy F. Hobson & Julia H. Lehman (2020) A rapid, spatially dispersive frequency comb spectrograph aimed at gas phase chemical reaction kinetics, Molecular Physics, 118:16, e1733116, DOI: 10.1080/00268976.2020.1733116

To link to this article: https://doi.org/10.1080/00268976.2020.1733116

MOLECULAR PHYSICS
2020, VOL. 118, NO. 16, e1733116 (9 pages)
https://doi.org/10.1080/00268976.2020.1733116

Taylor & Francis
Taylor & Francis Group

NEW VIEW

A rapid, spatially dispersive frequency comb spectrograph aimed at gas phase chemical reaction kinetics

Frances C. Roberts [a], H. J. Lewandowski [a,b], Billy F. Hobson [a] and Julia H. Lehman [a]

[a]School of Chemistry, University of Leeds, Leeds, UK; [b]JILA and Department of Physics, University of Colorado and the National Institute of Standards and Technology, Boulder, CO, USA

ABSTRACT

This New Views article will highlight some recent advances in high sensitivity gas detection using direct infrared absorption frequency comb laser spectroscopy, with a focus on frequency comb use in chemical reaction kinetics and our own contribution to this field. Our recently implemented detection technique uses a combination of a 12.9 GHz free spectral range virtually imaged phased array and diffraction grating to spatially disperse the mid-infrared frequency comb onto a camera. Individual frequencies or 'comb teeth' of a 250 MHz repetition-rate frequency comb are able to be resolved. High molecular sensitivity is achieved by increasing the interaction path length using a Herriott multipass cell. High spectral resolution, broadband spectral coverage, and high molecular sensitivity are all achieved on an adjustable 1–50 µs timescale, making this frequency comb apparatus ideal for measuring chemical reaction kinetics where multiple absorbing species can be monitored simultaneously. This New Views article will also discuss some of the challenges and decisions that chemists might face in implementing this advanced physics technology in their own laboratory.

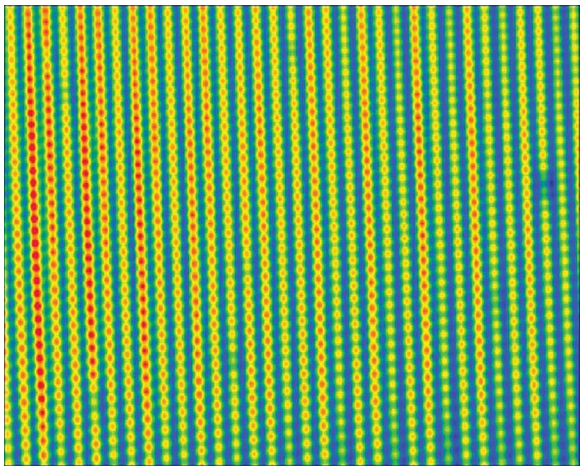

Spatially dispersed 250 MHz mid-infrared frequency comb laser, with absorption of some frequencies by a dilute sample of methane.

ARTICLE HISTORY
Received 16 October 2019
Accepted 10 February 2020

KEYWORDS
Frequency combs; chemical kinetics; trace gas detection

Introduction

Over the last two decades, frequency comb lasers have been developed and used primarily by physicists [1]. This is partly because a considerable amount of optical system expertise is needed to build such a laser. The result was that these lasers were applied to mostly physics-type studies such as ultra-precise metrology and calibration of astronomical measurements [2,3]. While many chemistry applications have begun to be explored using frequency comb lasers, such as those highlighted in recent reviews [4–11], now that commercial 'turn-key' frequency comb laser systems can be purchased at

CONTACT Julia H. Lehman j.lehman@leeds.ac.uk

various wavelengths, there is a great opportunity for the wider chemical community to engage with this optical physics technology.

Frequency comb lasers are a simultaneously broadband and high-resolution light source generated by the phase stabilisation of a mode-locked femtosecond laser. Although these lasers have been most often designed for near-infrared wavelengths, partially because of convenient wavelength fibres operating near 1560 nm or 1040 nm, frequency comb lasers have begun to be extended into the mid-infrared wavelength range where there are many vibrational transitions of chemically important functional groups extending to the 'fingerprint region' of the spectrum. Operating in these regions of the spectrum is beneficial in chemistry since fundamental vibrational frequencies have at least an order of magnitude larger oscillator strength compared to vibrational overtones accessible in the near infrared. This increases the potential detection sensitivity in direct absorption spectroscopy measurements, allowing the technology to progress further into trace gas detection and monitoring of transient chemical phenomena.

From a chemist's perspective, one of the largest advantages of this light source is due to its high resolution and broad spectral coverage. As demonstrated in a number of proof-of-principle, high-impact experiments, frequency comb lasers excel in trace gas detection, high resolution molecular spectroscopy, and chemical reaction kinetics [12–19]. The impacts of this new capability are already being felt in atmospheric and combustion monitoring [20–23]. These lasers can also be implemented in breath gas analysis and in laboratory settings for monitoring chemical reaction kinetics [12,19,24,25]. There are several excellent reviews highlighting some of these achievements [4–11].

Combining frequency comb lasers with rapid detection of many frequency components using spatially dispersive optics creates a spectrometer with many advantages for chemically important studies. One main advantage of using frequency comb lasers for direct absorption measurements is the short timescale over which an experiment can be completed due to the nature of the light itself. The high throughput, or experimental velocity, is a result of being able to measure a spectrum with high resolution and over a large bandwidth simultaneously. To achieve a similar broadband, high-resolution spectrum with a narrowband single frequency laser, one would need to scan the laser over a wide frequency range. Using a frequency comb laser decreases the experimental timescale, and thus reduces the impact of long timescale drifts or fluctuations (such as power, temperature, or other experimental considerations) on the overall data collection.

A second advantage, which directly impacts the suitability of using frequency combs for studying chemical reaction kinetics, is the minimum time resolution possible with this spectrometer. The time resolution of the spectrometer is the time it takes for a *single* (not averaged) broadband, high resolution spectrum to be collected, and is determined mainly by the detection method. For example, the time resolution of spatially dispersive spectrometers are typically limited by the minimum camera exposure (or integration) time. Microsecond camera exposure times can be reached in the mid-infrared, which is the case for our spectrometer discussed below, while still yielding a broadband, high resolution infrared spectrum [12,25]. Near infrared cameras can achieve even shorter exposure times. The short exposure times are particularly useful in chemical reaction kinetics. Multiple products can be identified within a single broadband high-resolution spectrum, and the timescale of their appearance monitored concurrently with the disappearance of a reactant. Multiplexed or coupled information on reaction rate coefficients can then be derived. The time resolution of time domain methods, such as dual-comb spectroscopy or Fourier transform spectrometers, are often slower by at least an order of magnitude. To the best of our knowledge, the fastest dual-comb spectrometer, which spans a similar broad spectral bandwidth (5 THz or 166 cm^{-1}) with similar resolution (204 MHz or 0.007 cm^{-1}) compared to the spatially dispersive spectrometer, has been able to reach approximately 700 μs [23]. Faster, sub-microsecond time resolutions are also possible, but often at the expense of spectral coverage or resolution, and will be discussed further below. However, these instruments show significant promise for liquid-phase kinetics measurements. It should be noted that we are specifically discussing *direct* (linear absorption) frequency comb measurements. *Indirect* (non-linear) frequency comb spectroscopies are able to reach even faster timescales [26–30].

This New Views article will present our own contribution to the field of direct absorption infrared frequency comb spectroscopy for measuring chemical reaction kinetics. Here, we exploit the simultaneously broadband, high-resolution light source coupled to a spatially dispersive detection scheme featuring microsecond time resolution, enabling its use in chemical reaction kinetics. This article will also discuss some of the challenges and decisions that chemists might face in implementing this advanced optical physics technology in their own chemistry laboratory.

Our contribution

Experimental methods

Our experiment uses a frequency comb laser system from Menlo Systems, which employs difference frequency generation (DFG) to produce a mid-infrared (2700–3300 cm^{-1} or 3000–3500 nm) frequency comb laser [31,32]. An Er-doped fibre laser (1560 nm) is the master frequency comb laser and has a repetition rate (f_{rep}) of 250 MHz, which is the frequency spacing between adjacent comb teeth. The f_{rep} is tuneable over a ± 500 Hz range and is stabilised using a 10 MHz rubidium clock frequency standard (SRS FS725).

The Er fibre master frequency comb laser has two outputs, one of which is at 6400 cm^{-1} (1560 nm) and is directly amplified. The other output is frequency shifted to 9600 cm^{-1} (1040 nm) and then amplified. The 6400 and 9600 cm^{-1} amplified outputs are spatially and temporally overlapped in a periodically poled lithium niobate (PPLN) nonlinear crystal and undergo DFG to produce the 3100 cm^{-1} (3200 nm) output of the full laser system (approximately 120 mW, 80 fs pulse width). The bandwidth of the laser output is nominally 600 cm^{-1}, peaking near 3100 cm^{-1}. Small shifts of the peak wavenumber (on the order of 100 cm^{-1}) and the relative intensity of the comb teeth over the bandwidth of the laser can be achieved by tuning the PPLN temperature and the time delay between the 6400 and 9600 cm^{-1} outputs. The individual comb teeth frequencies of the laser output are described by $f_n = nf_{rep} + f_{ceo}$, where f_{ceo} is the carrier envelope offset frequency. Since the 6400 and 9600 cm^{-1} outputs are generated from the same master frequency comb laser, $f_{ceo} = 0$.

The experimental setup of the laser and the rest of the optical system is shown in Figure 1a. The mid-infrared comb is coupled into and out of a Herriott multipass gas cell, where the light undergoes 18 passes achieving a total interaction path length of 430 cm. This path length is calibrated using a known quantity of methane and a spectral simulation [33], which uses the line strengths of the methane ν_3 vibrational band from HITRAN [34]. Upon exiting the Herriott cell, the laser is coupled into a single mode mid-infrared fibre. The fibre is used to both increase the flexibility of the optical path and spatially filter the laser beam. The enhanced beam quality out of the fibre helps achieve more consistent results from the imaging detection system.

The imaging detection system, which consists of two dispersive optical elements, an IR-sensitive camera, and a few lenses, is similar to Ref. [35] and begins at the output of the fibre (Figure 1). After the output of the fibre, the laser beam is collimated and expanded to a beam diameter of approximately 1 cm. The beam is then focussed using a cylindrical lens (100 mm focal length)

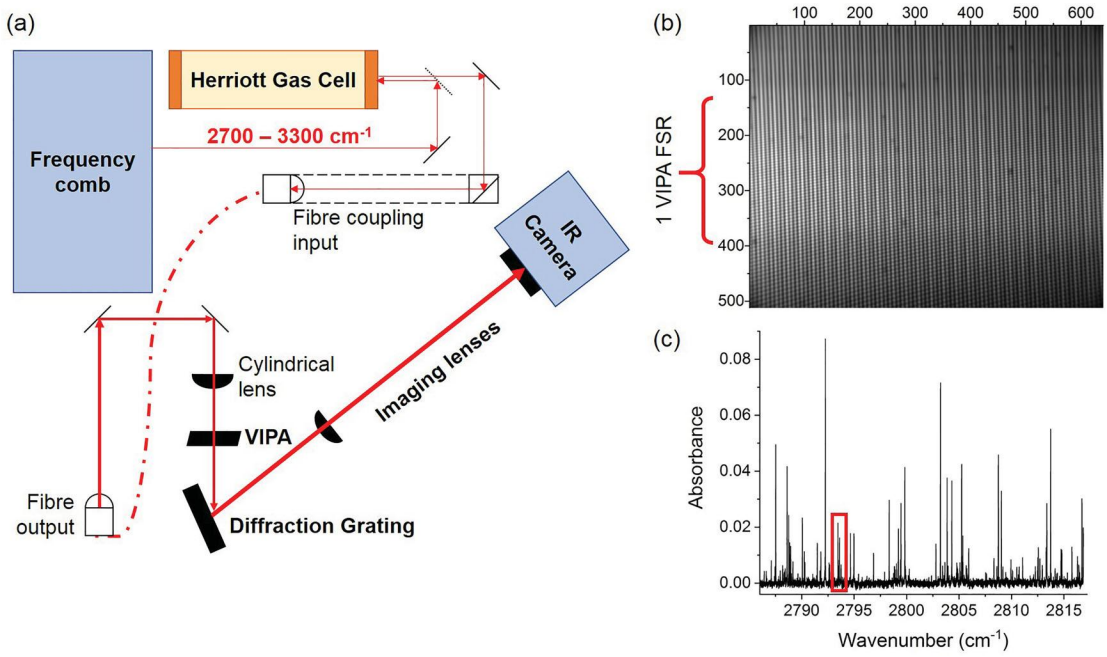

Figure 1. (a) Experimental setup, with important optical elements highlighted. (b) Greyscale image of a spatially dispersed frep = 250 MHz frequency comb on a 512 x 640 pixel InSb array camera, using a 50 µs exposure time and averaged for 190 images. Absorptions due to methane present in the gas cell (0.65% CH_4 in N_2 in 9.1 mbar total pressure) are seen as an attenuation of the light. The vertical spatial coverage of one VIPA FSR (51 comb teeth) is marked on the left. (c) Absorption spectrum resulting from interleaving 10 different frep images, one of which is panel (b). The red box indicates the region of the spectrum detailed in Fig. 3.

into the entrance of a virtually imaged phased array (VIPA, Light Machinery). A VIPA is essentially a tilted etalon that converts the input laser beam to a series of vertical parallel outputs, which constructively interfere at a set angle depending on the wavelength of the light [36]. In essence, the VIPA provides a repeating 'filter' of 12.9 GHz (0.43 cm^{-1}), which is the free spectral range (FSR). Since each mode order of the VIPA is spatially overlapped, the spectrometer requires a second dispersive element to spatially separate each mode. To accomplish this, we use the first order diffraction from a mid-infrared blazed diffraction grating (450 lines per mm, Laser Components). The total power per comb tooth is approximately 1 nW incident on the infrared camera.

The spatially dispersed frequency comb, which is now a 2D array of comb teeth, is imaged onto a mid-infrared camera (Infratec, InSb array, 512×640 pixels, 15 µm pixel pitch, Stirling cooled). An example image is shown in Figure 1b. The camera has a variable repetition rate up to 125 Hz at full frame, with a minimum camera frame exposure time of 1 µs. The data presented here showcase the 5 µs and 50 µs camera exposure times as representative results from this spectrometer. LabVIEW software controls the data acquisition, including a digital timing generator that triggers the camera exposure and the frequency generator that sets the laser repetition rate. MATLAB code is used to analyse the data, converting 2D array images of light intensity into absorption spectra as a function of wavenumber (Figure 1c). In order to transform the image into an absorption spectrum, each vertical column is truncated to 1 VIPA FSR (51 frequency comb teeth, which appear as 'dots') and then concatenated with the next horizontally displaced column. The integrated intensities of each comb tooth are measured with a gaseous sample present ('signal') and without a sample present ('background'). The signal and background images are transformed into spectra, and the absorption spectrum is determined using the Beer–Lambert Law, $\frac{I(\nu)}{I_0(\nu)} = \exp(-n\sigma(\nu)L)$, where $I(\nu)$ is the signal spectrum, $I_0(\nu)$ is the background spectrum, n is the concentration (molecules cm^{-3}), $\sigma(\nu)$ is the absorption cross section (cm^2 $molecule^{-1}$), and L is the path length (cm). An example of a spectrum created from this analysis of an image (Figure 1b) is shown in Figure 1c.

Since the spacing between adjacent comb teeth is 250 MHz (0.0083 cm^{-1}), the laser repetition rate must be scanned in order to observe absorptions occurring at frequencies between comb teeth. We scan the repetition rate between 249.9995 MHz – 250.0004 MHz using a step size of 100 Hz to measure 10 different spectral images. The images corresponding to each f_{rep} step are analysed separately and their spectra are interleaved to produce the final absorption spectrum. The spacing between adjacent data points in the final interleaved absorption spectrum is approximately 0.001 cm^{-1} (30 MHz). This can be calculated using $f_n = nf_{rep}$, where n is approximately 335,000 in the mid-infrared near 2800 cm^{-1}.

Results and discussion

Using a commercial mid-infrared frequency comb and our optimised VIPA-grating-camera (VGC) detection system, we are able to measure individually resolved comb teeth, which represents a significant advancement in frequency comb imaging. Using the combination of a $f_{rep} = 250$ MHz comb, 12.9 GHz FSR VIPA, and 450 lines per mm blazed diffraction grating, individual comb teeth are resolved in the image. Typically, an external cavity filter using a Vernier multiple of the repetition rate is used to increase the spacing between imaged comb teeth, which is effectively like increasing the repetition rate of the laser [18,35,37]. In this work, an external cavity filter is not needed in order to resolve individual comb teeth, which reduces the apparatus complexity. This is the first time, to the best of our knowledge, where individual comb teeth have been resolved for laser repetition rates below 2 GHz [35,38,39]. Figure 2 showcases the resolution of our VGC spectrometer, and includes an intensity profile along one vertical stripe of comb teeth in the image. Representative Gaussian fits to several of the comb teeth along this vertical stripe are shown, and have a full-width-at-half-maximum (FWHM) of approximately 4.2 pixels. Approximately 5.5 pixels separate the peak of one comb tooth from the next, resulting in a spectrometer resolution of 190 MHz, which is smaller than the comb tooth spacing of 250 MHz. This is over two times lower than the recently reported 460 MHz resolution dispersive frequency comb spectrometer in the far infrared [38]. In Figure 2, it can be seen that the minimum intensity between peaks in the vertical profile is approximately 35% lower than the maximum intensity of the peaks, exceeding the definition criterion for peaks to be resolved [40]. Each comb tooth is not resolved to baseline in the vertical direction (VIPA resolution). This manifests itself as a slightly broadened instrument lineshape function (see below).

The performance of the VGC was tested using a low concentration of methane in the Herriott multipass gas cell (0.65% CH_4 in N_2, total pressure 9.1 mbar, total path length 430 cm). When methane is present in the gas cell, it absorbs some of the frequencies of the frequency comb laser. This is seen on the camera as a reduction in light intensity at a specific location, as shown in Figure 1b and, more obviously, in Figure 2. One full image contains approximately 3,700 unique frequency comb teeth,

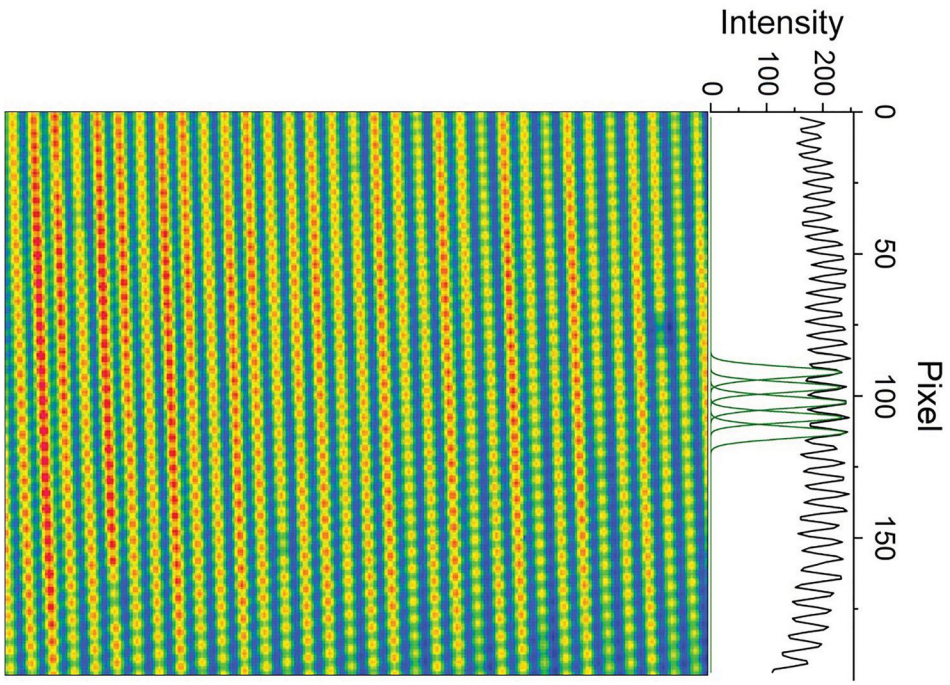

Figure 2. Zoomed in image, approximately 200 x 250 pixels, of the infrared frequency comb near 2800 cm^{-1} after adding a sample of dilute methane to the gas cell. Each dot in the image is a different frequency comb tooth with $f_{rep} = 250$ MHz. The image shows approximately 1200 unique frequencies. The dots with attenuated intensity are frequencies that have been absorbed by the methane sample. A representative intensity profile through the vertical dimension of the image is shown to the right, with Gaussian fits to several of the comb teeth.

each spaced by 250 MHz (0.008 cm^{-1}), and represents a 900 GHz (30 cm^{-1}) wide snapshot of a high-resolution infrared spectrum. To obtain a full spectrum, ten different repetition rates of the laser are used resulting in ten sets of images totalling a measurement of 37,000 unique frequencies. These result in data points in the final spectrum spaced by approximately 0.001 cm^{-1}, as discussed previously. The frequency window imaged by the camera is set by the angle of the diffraction grating with respect to the incoming light from the VIPA. The size of the detector array limits the range of frequencies captured in one image, as the size of the beam is larger than the detector. However, different frequency ranges can be imaged by changing the angle of the diffraction grating. By concatenating spectra at different grating angles, we can obtain a full spectrum over the entire bandwidth of the laser.

To calibrate the frequency axis of a full spectrum, a sample with a known infrared absorption spectrum is placed in the Herriott cell. In our experiment, we use the ν_3 vibrational band of methane and comparison data from the HITRAN database for this calibration [34]. A comparison of the analysed images with the known spectrum of methane allows for the sequential integer numbers n to be determined for each frequency comb tooth in the image, yielding an absolute frequency x-axis using the equation $f_n = nf_{rep}$. Using many absorption lines for methane uniquely defines n for each comb tooth. Therefore, the centre frequency of each comb tooth has an accuracy limited by the rubidium frequency clock, which sets the repetition rate. A portion of the methane spectrum, with the calibration applied, can be seen in Figure 3 for a camera exposure of 50 µs and an average of 190 images (9.5 ms total integration time, equating to approximately 1.5 s in real experiment time using a camera repetition rate of 125 Hz). Several methane transitions are observed over this 0.5 cm^{-1} window, along with the baseline noise typical of the averaged full spectrum. A simulation of the absorption spectrum using the HITRAN Application Programming Interface (HAPI) is overlaid as the red curve [33]. This simulation accounts for the temperature, pressure, path length, and concentration of the methane mixture. An additional instrument linewidth broadening function must be used to match the experimental linewidths, which have an approximate FWHM of 0.015 cm^{-1}. The additional breadth is most likely due to the separation of the comb teeth in the vertical dimension not being fully resolved to baseline. This results in Lorentzian instrument lineshape function [41].

A figure of merit called a noise equivalent absorption (NEA) is used to compare system performances. The NEA is a function of the standard deviation of the baseline noise level (σ) measured over an integration time (T)

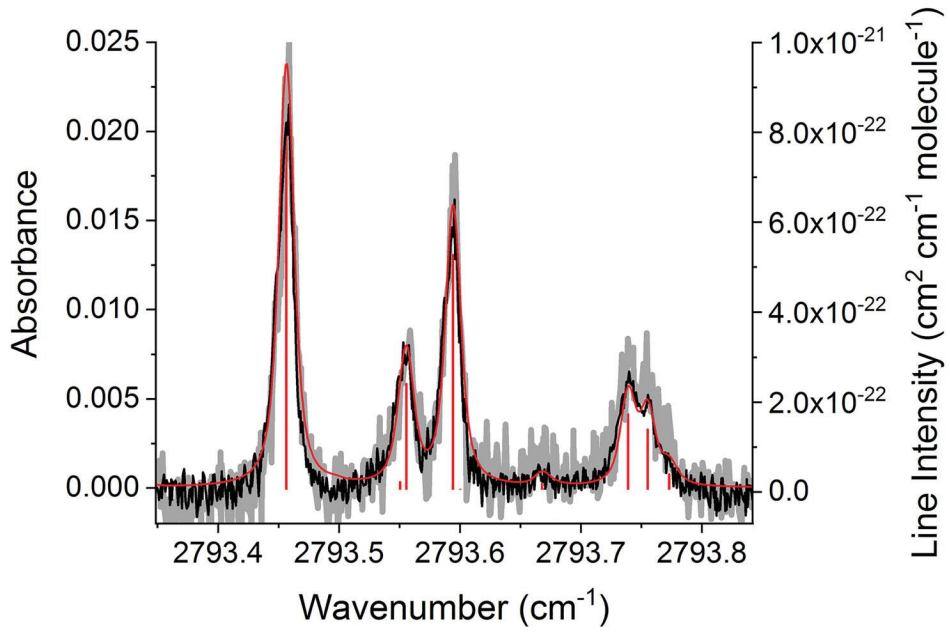

Figure 3. Subset of the experimental methane absorption spectrum (black trace, left y-axis) spanning approximately 0.5 cm^{-1} taken from the trace shown in Figure 1c enclosed in the red box. The sample is a gas mixture where $[CH_4] = 1.44 \times 10^{15}$ molecules cm^{-3}, or 0.65% CH_4 in N_2 in 9.1 mbar total pressure. A simulated CH_4 spectrum (red trace) is overlaid, also using the same left y-axis, and is discussed further in the text. Spectral line intensities from the HITRAN database (red sticks) are plotted against the right y-axis, and are arbitrarily scaled compared to the left y-axis. The grey lines show the experimental methane absorption spectrum using a 5 µs time resolution instead of the 50 µs time resolution, averaged for the same number of images, which corresponds to the same amount of laboratory time.

for a pathlength (L). In our experiment, σ has been measured for the full spectrum resulting from an f_{rep} scan with 10 steps, with each 50 µs image actively integrated for 9.5 ms. Thus, normalising to a 1 s integration time, $NEA^{1s} = \frac{\sigma}{L}\sqrt{T} = 9.8 \times 10^{-8} cm^{-1} Hz^{-1/2}$. For a shorter time resolution, such as a 5 µs camera exposure time actively integrated for a shorter 950 µs, $NEA^{1s} = 1.0 \times 10^{-7} cm^{-1} Hz^{-1/2}$. Note that the same number of camera images are used in the calculation of these two NEA^{1s} measurements. A visual representation of the increase in baseline noise in using a 5 µs time resolution compared to a 50 µs time resolution is shown in Figure 3. The instrument NEA^{1s} values are on-par with the system performance values listed in Table 5 of Ref. [4], which compares a variety of spectrometers using incoherent and coherent light sources for broadband spectroscopy. For example, a Fourier transform spectrometer using a frequency comb laser with a centre wavenumber of 2660 cm^{-1} (3760 nm) in a high finesse cavity has a $NEA^{1s} = 5.5 \times 10^{-9} cm^{-1} Hz^{-1/2}$ [42]. Similarly, for a frequency comb laser centred near 2680 cm^{-1} (3730 nm) coupled to a high finesse cavity and detected using a VGC spectrometer, $NEA^{1s} = 4.8 \times 10^{-8} cm^{-1} Hz^{-1/2}$ [43]. Undoubtedly, there have been further advancements in frequency comb detection techniques that have decreased NEA^{1s} since that review in 2017 [44].

Although NEA^{1s} is a useful figure of merit to compare different systems, a minimum detectable concentration of methane can also be calculated for our system to put this into a broader chemical context. Using a detectable absorption defined by 3σ above our baseline noise and methane absorption line intensity values of 1×10^{-19} cm^2 cm^{-1} $molecule^{-1}$, a minimum methane concentration of approximately 8×10^{11} molecules cm^{-3} is detectable in our system using a 50 µs time resolution actively integrated for 9.5 ms. Using a 5 µs time resolution actively integrated for 950 µs, a minimum observable methane concentration is approximately 2.5×10^{12} molecules cm^{-3}. In this analysis, we chose to use the stronger line strengths near the centre of the ν_3 vibrational band, rather than the much smaller line strengths at the edge of the ν_3 vibrational band shown by the red sticks in Figure 3 [34]. This minimum observable concentration is comparable to, or lower than, the concentrations used in many gas phase kinetics experiments, where concentrations of reactants are typically on the order of 10^{13} molecules cm^{-3} and product concentrations can be on the order of 10^{12} molecules cm^{-3} or lower. Of course, given that methane is a strong infrared absorber with a large line strength compared to other molecules, further improvements are ongoing to improve the sample interaction path length in order to measure trace

amounts of gaseous molecules with smaller infrared line intensities.

Challenges in comb implementation: critical design decisions

Frequency comb lasers have the potential to become a powerful optical tool in the chemist's toolbox. As a simultaneously broadband and high-resolution technique, the use of frequency combs in direct absorption spectroscopy has benefits over single frequency scanning absorption methods and incoherent light source Fourier Transform spectroscopy methods. However, there are challenges in working with frequency comb lasers, some of which still need to be overcome in order to see their full integration into the broader scientific community. As a new lab and particularly a lab situated outside of a physics department, we are in a unique position to comment on some of things to consider when making experimental design decisions.

The first decision is whether to build or purchase the laser system itself. Assuming that a chemist is more interested in the application of the frequency comb laser to chemistry questions rather than building the laser system, purchasing a system is likely the more appropriate choice considering the cost–time trade-off. There are a wide range of commercial frequency comb lasers becoming available. Potential users are encouraged to consider repetition rate, wavelength, power, and complexity for end users very carefully before investing in this equipment. These choices are also inherently coupled to the desired detection method. While stable frequency comb lasers can be purchased for prices similar to a pulsed Nd:YAG laser, the cost can become increasingly expensive if the system is designed to produce high optical power at wavelengths away from the near infrared fundamental wavelengths of Er or Yb doped fibre lasers. A tuneable laser wavelength or broader spectral coverage will likely come at an additional cost and with added complexity for the user. However, our choice of a DFG-based frequency comb negated some of this complexity since f_{ceo} for the mid-infrared output is zero, and thus there is no need for complex f_{ceo} stabilisation components.

The choice of a detection system is the next important decision for potential new users. To take advantage of the high resolution and broadband nature of this light source, a user could spatially disperse the comb frequencies and collect each individual frequency comb tooth separately, as is done in our group with the VGC detection, or a user can operate in the time domain instead and use Fourier Transform methodologies or dual comb spectroscopy [45]. These time domain methods can also measure comb-tooth resolved spectra [45]. Vernier techniques are a still higher resolution alternative to the VGC cross dispersion optical setup [46,47], but as this method does not yet offer the time resolution of DCS or VGC detection, this method will not be discussed further. There are several excellent reviews highlighting the different detection techniques with their advantages and disadvantages [4,5,6,11], but we explicate some things to consider here.

Spatially dispersive methods are ideal for measuring chemical reaction kinetics because of the achievable time resolution and the high experimental throughput. Although the breadth of spectral coverage will be limited by the size of the detector array for any single image, the rapidity of measurements and ease of use can outweigh this potential disadvantage. With more time and technological developments, these disadvantages will likely be addressed. Using a VIPA has additional advantages in frequency resolution, where Hz-level precision has been reported for measurement of cavity resonances, and in frequency self-calibration possibilities [48,49].

In contrast, dual-comb spectroscopy (DCS) has potential advantages over spatially dispersive methods, although there are also several disadvantages. DCS can be thought of as a Fourier transform spectrometer with no moving parts. This has the potential for increased robustness and ability to be used in field environments, which is an attractive option for atmospheric scientists. As the name implies, two frequency comb lasers operating at slightly different repetition rates are necessary for this technique, which increases the system cost and size. However, newer techniques are being developed to use a single free-running laser [50], and there is work on miniaturising these systems [51]. More information on the development of DCS methods can be found in a recent review [11]. Although the time domain detection technique used in DCS has advantages similar to FTIR, there is also a disadvantage in the experimental time resolution. This is currently limited to approximately 700 μs for a similarly broadband (5 THz or 166 cm^{-1}) and high resolution (204 MHz repetition rate) spectrum compared to the spatially dispersive spectrometer, which is too slow for use in measuring some gas-phase chemical reaction kinetics and currently has lower molecular sensitivity [23]. Microsecond or faster time resolution is possible in DCS, sometimes using quantum cascade lasers (QCLs), but often achieve this time resolution at the expense of spectral bandwidth or resolution [52–54]. For example, a time resolution of 13 μs was achieved over an approximately 60 GHz (2 cm^{-1}) spectral bandwidth with 300 MHz (0.01 cm^{-1}) resolution [54]. While this is an excellent example of the capabilities of dual comb spectroscopy, there is still improvement that would be

necessary in order to reach the broad spectral bandwidth while maintaining high resolution compared to the spatially dispersive frequency comb spectrometer. Indeed, a very recent example of DCS applied to gas-phase chemical reaction kinetics features a 120 μs time resolution with a broad spectral bandwidth (approximately 9 THz or 300 cm^{-1}) and 6 GHz (0.2 cm^{-1}) resolution [19].

Both of the above detection techniques require home built optical setups, and data collection and analysis code. However, fully coupled frequency comb laser and detection systems are just beginning to be commercially available, offering a turn-key system for immediate use in chemistry. For example, IRsweep has produced a benchtop FTIR system based on dual-comb spectroscopy using high repetition rate QCL combs and offers sub-microsecond time resolution [52]. Since this system uses a coherent light source, there are additional advantages over traditional step-scan FTIR spectrometers despite covering a narrower spectral range. However, again, the microsecond or sub-microsecond time resolution is achieved at the expense of spectral resolution (0.33 cm^{-1} for 1 μs and 8 cm^{-1} for 1 ns) making it more effective for solution-phase rather than gas-phase chemical kinetics.

Conclusions

In this New Views article, we discuss the design and implementation of a new mid-infrared frequency comb spectrometer. This is the first spatially dispersive spectrometer to resolve individual comb teeth of a frequency comb laser with a repetition rate below 2 GHz [35,38,39]. Even with a relatively uncomplicated Herriott multipass cell, with a total path length of 430 cm, the noise equivalent absorption and minimum detectable methane concentrations in this spectrometer show significant promise for use in highly sensitive gas detection. In addition, the variable 1–50 μs time resolution of the spectrometer makes it a very attractive option for use in gas-phase chemical reaction kinetics studies. To encourage the implementation of frequency combs in more chemical studies, we also discussed some of the decisions and opportunities for chemists in implementing frequency comb spectroscopy in their lab.

Disclosure statement

No potential conflict of interest was reported by the author(s).

Funding

This work was supported by funding from the 10.13039/10001 0665 H2020 Marie Skłodowska-Curie Actions (743642), EPSRC (EP/R01518X/1 and EP/R513258/1), the US-UK Fulbright Commission, University of Leeds, and the National Science Foundation (PHY-1734006).

ORCID

Frances C. Roberts http://orcid.org/0000-0002-2094-8785
H. J. Lewandowski http://orcid.org/0000-0002-0995-552X
Billy F. Hobson http://orcid.org/0000-0002-4834-8810
Julia H. Lehman http://orcid.org/0000-0001-6610-6519

References

[1] D.C. Yost, Am. J. Phys. **85** (10), 733 (2017).
[2] C. Hagemann, C. Grebing, C. Lisdat, S. Falke, T. Legero, U. Sterr, F. Riehle, M.J. Martin and J. Ye, Opt. Lett. **39** (17), 5102 (2014).
[3] D.F. Phillips, A.G. Glenday, C.-H. Li, C. Cramer, G. Furesz, G. Chang, A.J. Benedick, L.-J. Chen, F.X. Kärtner, S. Korzennik, D. Sasselov, A. Szentgyorgyi and R.L. Walsworth, Opt. Express. **20** (13), 13711 (2012).
[4] K.C. Cossel, E.M. Waxman, I.A. Finneran, G.A. Blake, J. Ye and N.R. Newbury, J. Opt. Soc. Am B-Opt. Phys. **34** (1), 104 (2017).
[5] M.L. Weichman, P.B. Changala, J. Ye, Z. Chen, M. Yan and N. Picqué, J. Mol. Spectrosc. **355**, 66 (2019).
[6] N. Picque and T.W. Hansch, Nat. Photonics. **13** (3), 146 (2019).
[7] F. Adler, M.J. Thorpe, K.C. Cossel, J. Ye, E.S. Yeung and R.N. Zare, Annu. Rev. Anal. Chem. **3**, 175 (2010).
[8] Z.H. Du, S. Zhang, J.Y. Li, N. Gao and K.B. Tong, Appl. Sci.-Basel. **9** (2, (2019).
[9] M. Vainio and L. Halonen, Phys. Chem. Chem. Phys. **18** (6), 4266 (2016).
[10] A. Schliesser, N. Picqué and T.W. Hänsch, Nat. Photonics. **6**, 440 (2012).
[11] I. Coddington, N. Newbury and W.C. Swann, Optica. **3** (4), 414 (2016).
[12] B.J. Bjork, T.Q. Bui, O.H. Heckl, P.B. Changala, B. Spaun, P. Heu, D. Follman, C. Deutsch, G.D. Cole, M. Aspelmeyer, M. Okumura and J. Ye, Science. **354** (6311), 444 (2016).
[13] P.B. Changala, M.L. Weichman, K.F. Lee, M.E. Fermann and J. Ye, Science. **363** (6422), 49 (2019).
[14] M.J. Thorpe, K.D. Moll, R.J. Jones, B. Safdi and J. Ye, Science. **311** (5767), 1595 (2006).
[15] T. Ideguchi, A. Poisson, G. Guelachvili, N. Picque and T.W. Hansch, Nat. Commun. **5**, Artn 3375 (2014).
[16] K.C. Cossel, E.M. Waxman, F.R. Giorgetta, M. Cermak, I.R. Coddington, D. Hesselius, S. Ruben, W.C. Swann, G.W. Truong, G.B. Rieker and N.R. Newbury, Optica. **4** (7), 724 (2017).
[17] G.B. Rieker, F.R. Giorgetta, W.C. Swann, J. Kofler, A.M. Zolot, L.C. Sinclair, E. Baumann, C. Cromer, G. Petron, C. Sweeney, P.P. Tans, I. Coddington and N.R. Newbury, Optica. **1** (5), 290 (2014).
[18] S.A. Diddams, L. Hollberg and V. Mbele, Nature. **445** (7128), 627 (2007).
[19] M.A. Abbas, Q. Pan, J. Mandon, S.M. Cristescu, F.J.M. Harren and A. Khodabakhsh, Sci. Rep. **9**, 17247 (2019).
[20] S. Coburn, C.B. Alden, R. Wright, K. Cossel, E. Baumann, G.W. Truong, F. Giorgetta, C. Sweeney, N.R. Newbury, K. Prasad, I. Coddington and G.B. Rieker, Optica. **5** (4), 320 (2018).

[21] L. Nugent-Glandorf, F.R. Giorgetta and S.A. Diddams, Appl Phys B-Lasers O. **119** (2), 327 (2015).

[22] G. W. Truong, E. M. Waxman, K. C. Cossel, F. R. Giorgetta, W. C. Swann, I. Coddington, and N. R. Newbury, IEEE: presented at the Conference on Lasers and Electro-Optics (CLEO), San Jose, CA, 2016 (unpublished).

[23] A.D. Draper, R.K. Cole, A.S. Makowiecki, J. Mohr, A. Zdanowicz, A. Marchese, N. Hoghooghi and G.B. Rieker, Opt. Express. **27** (8), 10814 (2019).

[24] M. Metsala, J. Breath Res. **12** (2), Artn 027104 (2018).

[25] M.J. Thorpe, D. Balslev-Clausen, M.S. Kirchner and J. Ye, Opt. Express. **16** (4), 2387 (2008).

[26] M.A.R. Reber, Y. Chen and T.K. Allison, Optica. **3** (3), 311 (2016).

[27] T. Ideguchi, S. Holzner, B. Bernhardt, G. Guelachvili, N. Picque and T.W. Hansch, Nature. **502** (7471), 355 (2013).

[28] A. Asahara and K. Minoshima, APL Photonics. **2** (4), 041301 (2017).

[29] J. Kim, B. Cho, T.H. Yoon and M. Cho, J. Phys. Chem. Lett. **9** (8), 1866 (2018).

[30] J. Kim, J. Jeon, T.H. Yoon and M. Cho, Chem. Phys. **520**, 122 (2019).

[31] S. Meek, A. Poisson, G. Guelachvili, T.W. Hansch and N. Picque, Appl Phys B-Lasers O. **114** (4), 573 (2014).

[32] F. Zhu, H. Hundertmark, A.A. Kolomenskii, J. Strohaber, R. Holzwarth and H.A. Schuessler, Opt. Lett. **38** (13), 2360 (2013).

[33] R.V. Kochanov, I.E. Gordon, L.S. Rothman, P. Wcisło, C. Hill and J.S. Wilzewski, J. Quant. Spectrosc. Radiat. Transfer. **177**, 15 (2016).

[34] I.E. Gordon, L.S. Rothman, C. Hill, R.V. Kochanov, Y. Tan, P.F. Bernath, M. Birk, V. Boudon, A. Campargue, K.V. Chance, B.J. Drouin, J.M. Flaud, R.R. Gamache, J.T. Hodges, D. Jacquemart, V.I. Perevalov, A. Perrin, K.P. Shine, M.A.H. Smith, J. Tennyson, G.C. Toon, H. Tran, V.G. Tyuterev, A. Barbe, A.G. Császár, V.M. Devi, T. Furtenbacher, J.J. Harrison, J.M. Hartmann, A. Jolly, T.J. Johnson, T. Karman, I. Kleiner, A.A. Kyuberis, J. Loos, O.M. Lyulin, S.T. Massie, S.N. Mikhailenko, N. Moazzen-Ahmadi, H.S.P. Müller, O.V. Naumenko, A.V. Nikitin, O.L. Polyansky, M. Rey, M. Rotger, S.W. Sharpe, K. Sung, E. Starikova, S.A. Tashkun, J. Vander Auwera, G. Wagner, J. Wilzewski, P. Wcisło, S. Yu and E.J. Zak, J. Quant. Spectrosc. Radiat. Transfer. **203**, 3 (2017).

[35] L. Nugent-Glandorf, T. Neely, F. Adler, A.J. Fleisher, K.C. Cossel, B. Bjork, T. Dinneen, J. Ye and S.A. Diddams, Opt. Lett. **37** (15), 3285 (2012).

[36] M. Shirasaki, Opt. Lett. **21** (5), 366 (1996).

[37] N.B. Hébert, S.K. Scholten, R.T. White, J. Genest, A.N. Luiten and J.D. Anstie, Opt. Express. **23** (11), 13991 (2015).

[38] K. Iwakuni, T.Q. Bui, J.F. Niedermeyer, T. Sukegawa and J. Ye, Opt. Express. **27** (3), 1911 (2019).

[39] L.C. Sinclair, K.C. Cossel, T. Coffey, J. Ye and E.A. Cornell, Phys. Rev. Lett. **107** (9), 093002 (2011).

[40] IUPAC, *Compendium of Chemical Terminology, 2nd ed. (the "Gold Book")* Compiled by A. D. McNaught and A. Wilkinson (Blackwell Scientific Publications, Oxford, 1997).

[41] X. Shijun, A.M. Weiner and C. Lin, IEEE J. Quantum Electron. **40** (4), 420 (2004).

[42] A. Foltynowicz, P. Maslowski, A.J. Fleisher, B.J. Bjork and J. Ye, Appl Phys B-Lasers O. **110** (2), 163 (2013).

[43] A.J. Fleisher, B.J. Bjork, T.Q. Bui, K.C. Cossel, M. Okumura and J. Ye, J. Phys. Chem. Lett. **5** (13), 2241 (2014).

[44] T.Q. Bui, P.B. Changala, B.J. Bjork, Q. Yu, Y.M. Wang, J.F. Stanton, J. Bowman and J. Ye, Mol. Phys. **116** (23–24), 3710 (2018).

[45] P. Maslowski, K.F. Lee, A.C. Johansson, A. Khodabakhsh, G. Kowzan, L. Rutkowski, A.A. Mills, C. Mohr, J. Jiang, M.E. Fermann, and A. Foltynowicz, Phys. Rev. A **93** (2), 021802 (2016).

[46] M. Siciliani de Cumis, R. Eramo, N. Coluccelli, G. Galzerano, P. Laporta and P.C. Pastor, J. Chem. Phys. **148** (11), 114303 (2018).

[47] F. Zhu, J. Bounds, A. Bicer, J. Strohaber, A.A. Kolomenskii, C. Gohle, M. Amani and H.A. Schuessler, Opt. Express. **22** (19), 23026 (2014).

[48] G. Kowzan, D. Charczun, A. Cygan, R.S. Trawiński, D. Lisak and P. Masłowski, Sci. Rep. **9** (1), 8206 (2019).

[49] G. Kowzan, K.F. Lee, M. Paradowska, M. Borkowski, P. Ablewski, S. Wójtewicz, K. Stec, D. Lisak, M.E. Fermann, R.S. Trawiński and P. Masłowski, Opt. Lett. **41** (5), 974 (2016).

[50] J. Chen, X. Zhao, Z. Yao, T. Li, Q. Li, S. Xie, J. Liu and Z. Zheng, Opt. Express. **27** (8), 11406 (2019).

[51] M.J. Yu, Y. Okawachi, A.G. Griffith, N. Picque, M. Lipson and A.L. Gaeta, Nat. Commun. **9**, 1869 (2018).

[52] J.L. Klocke, M. Mangold, P. Allmendinger, A. Hugi, M. Geiser, P. Jouy, J. Faist and T. Kottke, Anal. Chem. **90** (17), 10494 (2018).

[53] M. Yan, P.L. Luo, K. Iwakuni, G. Millot, T.W. Hansch and N. Picque, Light-Sci. Appl. **6**, e17076 (2017).

[54] G. Millot, S. Pitois, M. Yan, T. Hovhannisyan, A. Bendahmane, T.W. Hansch and N. Picque, Nat. Photonics. **10** (1), 27 (2016).